



Full length article



Fundamental links between shear transformation, β relaxation, and string-like motion in metallic glasses

Zhen-Ya Zhou^{a,b}, Yang Sun^c, Liang Gao^b, Yun-Jiang Wang^{d,e,*}, Hai-Bin Yu^{b,**}

^a School of Physics and Electronic-Electrical Engineering, Ningxia University, Yinchuan 750021, China

^b Wuhan National High Magnetic Field Center and School of Physics, Huazhong University of Science and Technology, Wuhan 430074, China

^c Department of Applied Physics and Applied Mathematics, Columbia University, New York, NY 10027, USA

^d State Key Laboratory of Nonlinear Mechanics, Institute of Mechanics, Chinese Academy of Sciences, Beijing 100190, China

^e School of Engineering Science, University of Chinese Academy of Sciences, Beijing 100049, China

ARTICLE INFO

Keywords:

Metallic glasses
Plastic deformation
relaxation
String-like motion
Accelerated molecular dynamics

ABSTRACT

Plastic deformation and relaxation dynamics are two major topics in glass physics. Secondary (β) relaxation has been assumed to be a relevant plastic mechanism in amorphous solids, e.g., metallic glasses (MGs), at the macroscopic scale. However, due to the constraints of the time scale of traditional computer simulation, it is still an open question whether the correlation can be justified at the atomic level, or is it just a correlation in a mean-field sense? In this work, molecular dynamics simulations augmented with metadynamics are conducted to study the basic atomic rearrangement mechanism up to experimentally relevant timescales (up to milliseconds). We show that in a unique $\text{Al}_{90}\text{Sm}_{10}$ MG with pronounced β relaxation, the atoms initiating the plastic deformation are exactly the ones apt to develop string-like cooperative motions, as expected from the perspective of β relaxation. For a $\text{Y}_{65}\text{Cu}_{35}$ MG without obvious β relaxation, string-like motions are rarely observed in the deformation of participating atoms, although their atomic displacements are also aligned in a correlative manner. Therefore, our laboratory long-time-scale observation enables the in situ construction of a fundamental link among the versatile concepts of shear transformation, β relaxation, and string-like motion in amorphous materials.

1. Introduction

Metallic glass (MG), also known as amorphous alloys [1–11], is of current interest and significance in condensed matter physics, materials science and engineering because of its unique structural features [12–18] and outstanding mechanical and functional properties. One of the enduring attractions of MGs is their interesting (and impressive) suite of mechanical properties [19–29]. However, the lack of macroscopic plastic deformation capacity at room temperature leaves MGs prone to catastrophic failure in load-bearing conditions, which becomes the Achilles' heel of MGs and hence restricts their possible widespread applications. Therefore, the plastic deformation of metallic glass below the glass transition temperature T_g has become a long-standing issue. It is well-known that the plastic deformation in the crystalline materials is accommodated by the motion of crystalline defects such as dislocations. In contrast, in MGs the plastic deformation is not allowed to be accommodated by dynamics of imperfections in crystalline materials [30–33]. The most widely accepted plastic rheological model in MGs is the shear

transformations (STs) concept [21,34–37]. Microscopically, the inelastic deformation of MGs is caused by the irreversible rearrangement of atoms in the ST regions. The formations and self-organizations of STs that induces the macroscopic shear bands in MGs [38]. The ST was originally defined in the deformation process by Argon [34], but it is now generally accepted that the ST is also closely related to the structure. Meanwhile, when the microscopic mechanism of structural excitation is not clear, this process is temporarily called ST (an event), which may include many deformation modes including string-like motions.

Meanwhile, it has long been recognized that the deformation behaviors of MGs are deeply rooted in their disordered structural features and the relaxation spectrum [39–50]. The localized flow event in MGs can be modeled as a thermally activated hopping between the neighboring inherent states after surmounting energy barrier in the potential energy landscape (PEL) [51,52]. In this framework, the key parameter of thermal activation is the energy barrier or activation energy. Based on the PEL theory, Johnson and Samwer proposed a cooperative shear model (CSM) to understand the deformation mechanism in MGs [53].

* Corresponding author at: State Key Laboratory of Nonlinear Mechanics, Institute of Mechanics, Chinese Academy of Sciences, Beijing 100190, China.

** Corresponding author.

E-mail addresses: yjwang@imech.ac.cn (Y.-J. Wang), haibinyu@hust.edu.cn (H.-B. Yu).

<https://doi.org/10.1016/j.actamat.2023.118701>

Received 12 July 2022; Received in revised form 7 January 2023; Accepted 10 January 2023

Available online 12 January 2023

1359-6454/© 2023 Acta Materialia Inc. Published by Elsevier Ltd. All rights reserved.

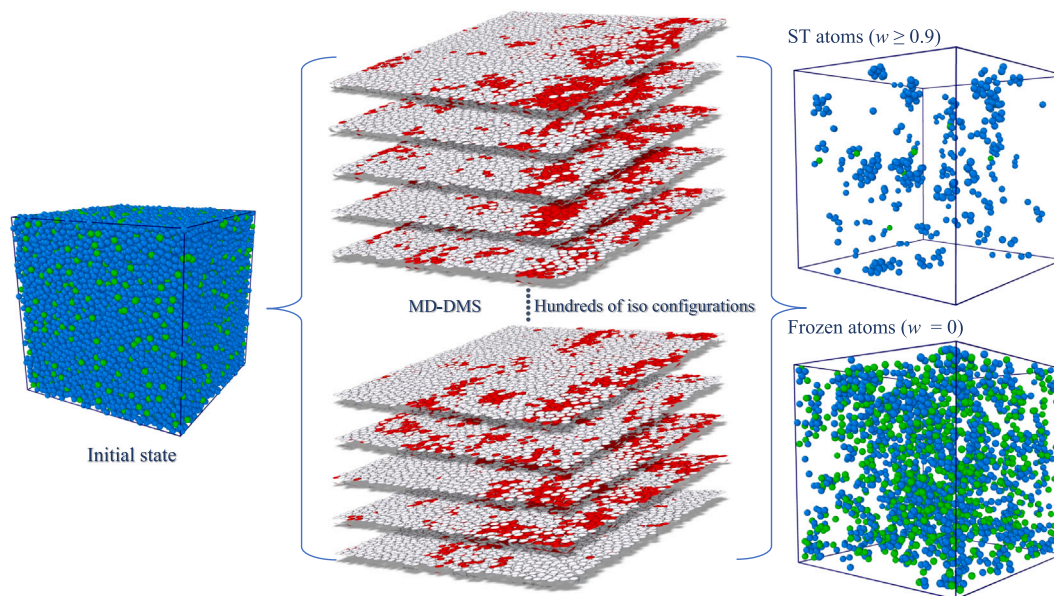


Fig. 1. (Color online) Schematic diagram of metallic glass iso configuration ensemble simulation.

It is suggested that the isolated flow units confined within the elastic matrix are associated with the β relaxation. Previous studies found direct experimental evidence that the activation energy of STs and β relaxation are nearly equivalent [41]. The results demonstrated that the plastic deformation and the β relaxation are directly correlated in MGs. However, the perceived relationships between these concepts are based on the correlation of the macroscopic experimental phenomena that are usually of mean-field sense, and no direct evidence is given so far with sufficient atomistic details. Moreover, some parameters, such as Poisson's ratio [20,54,55], free volume [56], β' relaxation [47], boson peak [44,45] and potential energy [57,58], are also correlated with mechanical properties of MGs. Despite these advances, a fundamental question remains open: what is the structural argument for the correlation between mechanical properties and various physics-informed parameters? To clarify this problem, it would be desirable to find some entity that matters deformation at atomic level. Can the β relaxation take up this challenging role?

To understand the nature of correlation between the β relaxation and plastic deformation, it is important to determine the specific atomic rearrangements in the β relaxation process. As early as the 1970s, β relaxation was known in polymer glass and considered to originate from the rotation of side chains and functional groups in polymer. Nevertheless, Johari and Goldstein discovered that β relaxation also exists in some rigid molecules without side chains or functional groups, indicating that some β relaxation must involve in the movement of the whole molecule rather than the degree of freedom within the molecule [59]. Recently, studies [60] have found that β relaxation in MGs originates from the string-like cooperative motions by classical molecular dynamics (MD) simulations at time scales of up to microseconds, which provides insights into the long-standing puzzle regarding the structural origin of β relaxations in metallic glasses. At the same time, for the string-like motion, it was found that thermal activation of string-like motion is present in both under-cooled liquids [61–63] and amorphous solids [64–69]. This string-like motion was also revealed by Rodney and Derlet et al. using the potential energy landscape exploration methods and their corresponding fluctuation time scale was estimated [40,70–72]. It is noteworthy that the athermally stress-driven STs arise from inflections in the PEL and that the core structure of such STs is more localized than the thermally-activated local structural excitations corresponding to the string-like motions [69].

To uncover the correlation between the β relaxation and plastic deformation, we seek to identify the elementary processes of specific ST

atomic clusters through atomistic simulations. The well-known bottleneck is that the temporal scale relevant to β relaxation and deformation at relatively low temperature is far beyond the reach of classical MD [73,74]. Here, we implement a metadynamics formulation that allows transition-state trajectories to be generated on appreciably longer timescales on the order of fractions of seconds [75]. Similar methods have been established and utilized to overcome the timescale limitation in simulating the structural relaxation, viscosity, crystallization, shear and creep deformation of disorder materials [40,70,76–80].

In this work, we used the so-called iso configuration ensemble to obtain the probability w of an atom participating in the ST. Then we conducted enhanced sampling of a local structural excitation with different w values in $\text{Al}_{90}\text{Sm}_{10}$ and $\text{Y}_{65}\text{Cu}_{35}$ MGs via well-tempered metadynamics (WT-MetaD) simulations [81–86] at the experimentally relevant temperature range ($T = 300, 440$ K) and the corresponding timescale, which is usually a forbidden regime for classical MD. We find that in $\text{Al}_{90}\text{Sm}_{10}$ MGs with obvious β relaxation, the atoms participating in plastic deformation are also those involved in the string-like coordinated motion, as predicted from β relaxation. For $\text{Y}_{65}\text{Cu}_{35}$ MG without obvious β relaxation, the plastic atoms do not form chain transport. These atoms might tend to form string-like motion in essence, but they are frozen by the surrounding immobile atoms. In summary, we used a combination of our three simulation methods of iso configuration ensemble, molecular dynamics dynamical mechanical spectroscopy (MD-DMS), and well-tempered metadynamics (WT-MetaD) to simulate each of the three deformation mechanisms, resulting in direct evidence with atomic fidelity of the correlation among β relaxation, string-like motions, and ST. We have not only demonstrated a fundamental link between the β relaxation, string-like motion and ST, but more importantly, the atomic mechanisms underlying the correlation are elucidated in a unified framework by means of different simulations protocols.

2. Methods

In this work, we combine a set of atomistic simulation and modeling techniques to reveal possible correlation between versatile concepts associated with the basic motion mechanisms of metallic glasses, which include the standard molecular dynamics to prepare glass samples, the MD-DMS (up to microseconds) to estimate the timescale of the β relaxation, the iso-configuration ensemble simulation to extract STs,

as well as the well-tempered metadynamics to assess the timescale of string-like motions relevant to experimental conditions. The combined simulations could shed light on establishing fundamental links between different structural excitation mechanisms.

2.1. Standard molecular dynamics

While all the simulations and modeling are performed by using the LAMMPS code [87–90], the details of MD simulations are explained below as a starting point for all the other simulation protocols. For the purpose of direct comparison, two distinct model glass systems, namely, $Y_{65}Cu_{35}$ and $Al_{90}Sm_{10}$, were selected and studied due to their different features of relaxation. They interact with an embedded-atom method potential constructed by Wang et al. [91], and a Finnis–Sinclair potential by Mendeleev et al. [92], respectively. These empirical potentials reproduce experimental results of relaxation features. The two glass models, containing 32 000 atoms, were obtained by continuous cooling from their equilibrium liquid state with a constant cooling rate of 10^8 K/s in the NPT ensemble (that is, constant number of atoms, pressure, and temperature). Such cooling rate is extremely slow in the framework of standard molecular dynamics. The external pressure was adjusted to fluctuate around zero during the quenching process by Parrinello–Rahman barostat. Periodic boundary conditions were applied in all the three directions. The classical MD time step $\Delta t = 2$ femtosecond. The change of potential energy during the cooling process is shown in Fig. S1 of the Supplemental Information (SI), which indicate noteworthy glass transition in both of the $Y_{65}Cu_{35}$ and $Al_{90}Sm_{10}$ metallic glasses.

2.2. Dynamical mechanical spectroscopy via MD

The dynamics of both the secondary β and primary α relaxations can be studied by an approach of MD-DMS simulations [60,93] that numerically reproduce the protocols of real DMS experiments. Specifically, at a temperature T , we applied a sinusoidal strain $\varepsilon(t) = \varepsilon_A \sin(2\pi t/t_\omega)$ varying with time, with a period t_ω (related to frequency $f = 1/t_\omega$) and a strain amplitude ε_A along the x direction of the model MG. Since the metallic glasses are of viscoelastic nature, there is phase difference Δ between the stress and strain. In this context, the resulting time-dependent stress $\sigma(t)$ is measured and fitted with an empirical form $\sigma(t) = \sigma_0 + \varepsilon_A \sin(2\pi t/t_\omega + \Delta)$. One example of the MD-DMS simulations is further demonstrated in Fig. S2 of SI. From a generalized Hooke's law, the loss modulus E'' is calculated according to $E'' = \sigma_A/\varepsilon_A \cos(\Delta)$. Here we used a strain amplitude of $\varepsilon_A = 0.6\%$ in all the MD-DMS simulations, which ensures that the deformation is in the elastic regime and structural evolution of the glass is neglected. In the MD-DMS simulations, NVT ensemble (that is, constant number of atoms, volume, and temperature) is applied. The cyclic strain–stress curves are obtained after tensile deformation. Specifically, at a given temperature like $T = 300$ K, a time-dependent tensile strain $\varepsilon(t) = \dot{\varepsilon} \cdot t$ with a constant strain rate ($\dot{\varepsilon} = 10^8$ s $^{-1}$) is applied along x direction. The resulting stress σ_x was recorded for the later analysis.

2.3. Iso-configuration ensemble simulations

The atoms which have participated in the shear transformations (STs) are recognized by the framework of the iso-configuration ensemble simulations. The ST events are not only related to the glassy structure but also have the randomness caused by thermal fluctuation. Even if being simulated from the same atomic structure, STs may take place at different atomic environment since the initial momentum is random guided by the Maxwell–Boltzmann distribution in a canonical ensemble. To get more accurate information about the STs in these two different systems, statistical analysis on activation probability is required. For the statistical purpose, we introduce the iso-configurational ensemble simulation proposed by Harrowell et al. [94,95], which consists of hundreds of independent simulation runs over a fixed time

duration. All the MD simulations start from the same configuration but with different initial condition (by assigning velocity randomly). This strategy allows to recognize the statistically meaningful STs compared with the usual loading protocol of the athermal quasi-static shear. The former method definitely contains more statistical information about ST than the latter which is more stress tensor specific and might miss some thermal activation component.

The details of the iso-configuration ensemble simulations are shown schematically in Fig. 1. Firstly, the initial configurations of glass samples at different temperatures are obtained by continuous cooling from liquid. At a specific temperature, hundreds of independent MD tensile tests are performed on the same glass configuration with equivalent initial conditions (but with velocity randomness). In all these tests, all the parameters for simulations are set identical except the initial velocities by Boltzmann–Maxwell distribution. After each iso-configuration ensemble simulation, we judge these atoms which have participated in the ST events if they experience the nonaffine squared displacement with magnitude larger than 40 \AA^2 . Thus, the specific atoms involved in the STs in each test can be obtained by analyzing the nonaffine atomic displacement. After statistical analysis, the probability of an atom being involved in any ST event can be calculated after all the equivalent deformations. Here we choose $w = N_{ST}/N_{All}$ to represent the probability of an atom participating in STs. N_{All} is the number of iso-configuration ensemble simulations, and N_{ST} denotes the times that this atom have taken part in the STs. Specifically, we define the atoms with higher w value ($w \geq 0.9$) as the ST atoms. The rest of atoms do not participate in ST events ($w = 0$) after all deformations are categorized to frozen atoms.

2.4. Well-tempered metadynamics

Once the ST atoms are selected by the iso-configuration ensemble simulations, one has the opportunity to estimate its timescale at lower temperature in the deep glassy state such as to shake hand with the β relaxation probed by MD-DMS. This is enabled by the well-tempered metadynamics samplings via the COLVARS package implemented in the LAMMPS code [96].

The WT-MetaD samplings are performed at two different temperatures, i.e., 300 K and 440 K, respectively. The timescale of the latter case (\sim microseconds) is available in the MD-DMS simulations such as we can compare the accelerated MD results with the direct, standard MD simulations. At each target temperature, the glass configuration is adopted from the cooling fragment with the memory of velocity information. The same configurations have been tested in the iso-configuration ensemble simulations to pick up the ST atoms. Such finite temperature models are further being equilibrated for 200 ps within an isothermal–isobaric ensemble before the metadynamics samplings. WT-MetaD samplings are then performed within the canonical ensemble with constant number of atoms, temperature and volume. After these operations, we guarantee the equivalent thermodynamic conditions of the metadynamics and standard MD simulations. Therefore, the results are not biased by human choices in the simulation parameters.

A key ingredient for the success of metadynamics samplings is the way of dimensionality reduction via suitable choice of an efficient collective variable (CV), which is capable of simplification of the $3N$ dynamics to one or two degrees of freedom. Note that, on the one hand, the local structural excitation in the form of either ST or string-like motion usually experiences essential nonaffine displacements. On the other hand, the root-mean-square displacement (RMSD) is metric of displacement that is similar to the non-affine squared displacement D_{min}^2 but it is easier to be implemented in the framework of metadynamics. Herein we use the RMSD of a group of ST atoms with respect to their reference positions as the CV of metadynamics, distinguishing

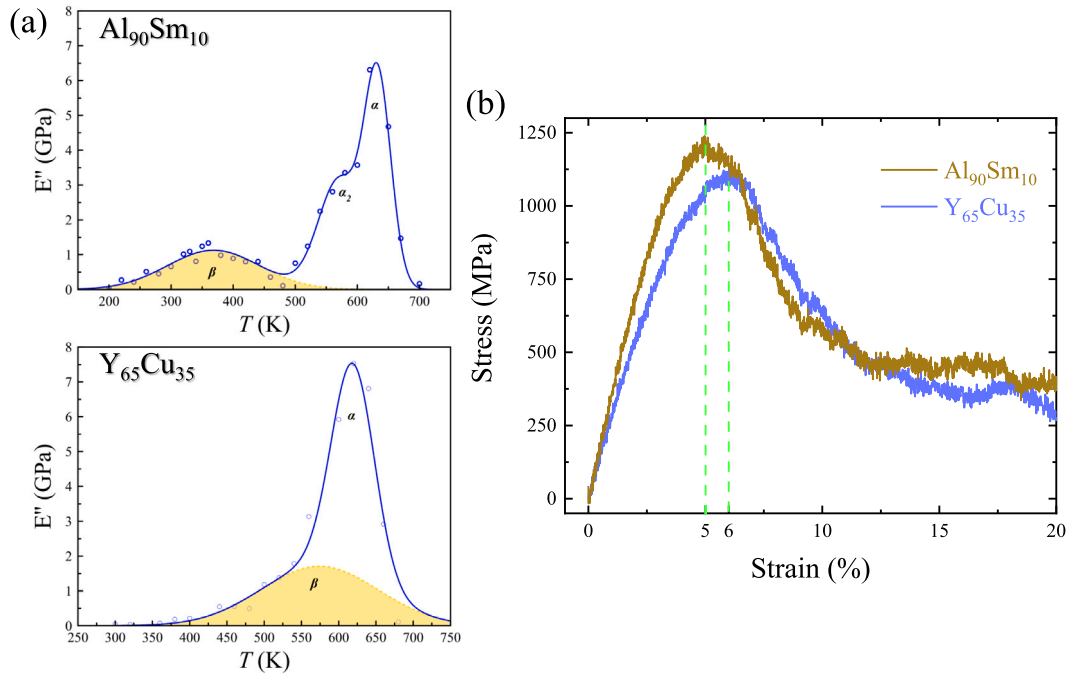


Fig. 2. (Color online) Relaxation and mechanical behaviors of two metallic glasses obtained by simulations. (a) Loss moduli E'' of $\text{Al}_{90}\text{Sm}_{10}$ and $\text{Y}_{65}\text{Cu}_{35}$ metallic glasses at oscillation period $t_\omega = 1 \mu\text{s}$. (b) Strain–stress curve of $\text{Al}_{90}\text{Sm}_{10}$ and $\text{Y}_{65}\text{Cu}_{35}$ metallic glass at constant strain rate $\dot{\epsilon} = 10^8 \text{ s}^{-1}$ and temperature $T = 300 \text{ K}$.

the energy minimum, saddle point, and the final configuration of a ST event. The RMSD is formulated as

$$\text{RMSD}(\{X_i(t)\}, \{X_i^{\text{ref}}\}) = \sqrt{\frac{1}{N} \sum_{i=1}^N \left| U [X_i(t) - X_{\text{cog}}(t)] - (X_i^{\text{ref}} - X_{\text{cog}}^{\text{ref}}) \right|^2}, \quad (1)$$

where N is the number of the sampled ST atoms. U represents an optimal rotation matrix from the reference coordinates X_i^{ref} to the instantaneous positions X_i at any sampling time t . $X_{\text{cog}}(t)$ and $X_{\text{cog}}^{\text{ref}}$ are the centers of geometry.

Once the CV is determined, the standard MD simulations is performed on all the atoms in the sample with canonical ensemble. During MD run, the trajectory of CV is recorded at each MD step with a resolution of 0.01 \AA . After every thousand MD steps (each step with time interval 2 fs), a bias energy in Gaussians are deposited as a function of CV varying with time. The WT-MetaD is a variant of the original metadynamics [82] which differs in the exact way of Gaussian depositions. In conventional metadynamics, the added Gaussians are invariant with time. However, in the WT-MetaD version, the Gaussian hills are rescaled at each MD step and, therefore, the bias potential is given with smaller magnitude as a function of time via

$$V(s, t) = \sum_{t'=0}^{t'<t} W \exp(-V(s(X(t')), t')/\Delta T) \times \exp\left(-\sum_{i=1}^d \frac{(s_i(X) - s_i(X(t')))^2}{2\sigma^2}\right). \quad (2)$$

Here $W = 0.01 \text{ eV}$ is the starting height of bias potential. s is the magnitude of CV, which is given by the instantaneous coordinate X . $\sigma = 0.2 \text{ \AA}$ is the width of the deposited Gaussian potential. i is the number of Gaussian depositions. This simple formula of the added Gaussians renders that the bias potential converges exactly and more smoothly [83].

A critical technique of the WT-MetaD sampling is the introduction of an artificial temperature ΔT augmented to the thermodynamic temperature T of a canonical ensemble. When running the WT-MetaD sampling in the long-time limit, the collective variable is evolved according to a modified temperature $T + \Delta T$. The bias potential adding rate is then gradually decreased according to $\dot{V}(s, t) = \omega \exp(-[V(s, t)/\Delta T]) \tau_G$, with $\tau_G = 2 \text{ ps}$ of 1000 MD steps and ω the initial bias deposition rate. $\Delta T = 1500 \text{ K}$ is used in this work. The artificial temperature does not alter the dynamics of all the atoms but only encourage the thermal fluctuation of CV. It properly boosts the CV dynamics and extends the sampling of physical time. Finally, we note that the artificial temperature ΔT is only a parameter of technique to control the deposition manner of Gaussian potentials. It definitely differs from the concept of the fictive temperature T_f in any glass-forming system that is familiar in the community of glass, which is used as a metric to quantify the degree of disorder in a disordered system such as glasses.

By keeping addition of bias potentials, the configuration is forced to escape from the original free energy basin of the CV. Finally, the FES is reconstructed by recalling the history of the added bias potentials as a function of s and the free energy barrier ΔG_2 is available. Thus, the frequency of a structural excitation, or a ST event, is estimated through the transition-state theory [97]

$$\nu = \nu_0 \exp\left(\frac{-\Delta G_2}{k_B T}\right), \quad (3)$$

with the attempt frequency ν_0 typically taken to be 10^{12} s^{-1} . In some cases, the attempt frequency may span multiple orders of magnitude [72]. However, we focus on the activation of atomic clusters with a few to a dozen of atoms, the attempt frequency does not fluctuate across multiple orders of magnitude because the number of atoms involved in calculating structural excitation does not change significantly in the present study. k_B is the Boltzmann's constant.

Considering the fact that the classical MD sampling (typically tens of millions of steps) has also filled part of the free energy basin, the final free energy barrier is accounted for both the natural thermal fluctuation (sampled by the classical MD) and WT-MetaD (via the bias potential),

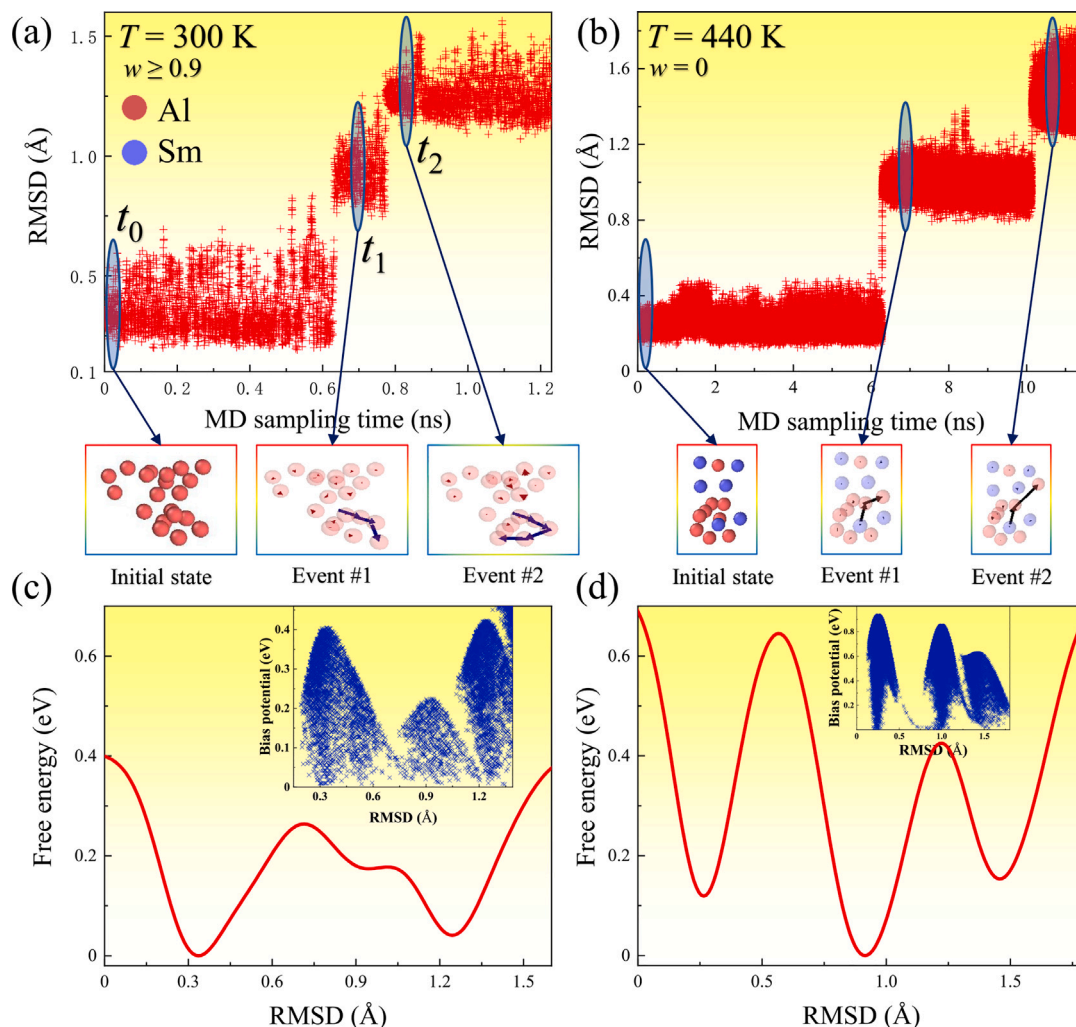


Fig. 3. Well-tempered metadynamics samplings of the accelerated atoms in $\text{Al}_{90}\text{Sm}_{10}$ metallic glasses. (a, b) Time evolution of RMSD. (c, d) Free energy profile versus RMSD. The inset shows the added bias potential. The middle panels show the initial state and patterns of the first two events, indicated by the sudden jump in RMSD. Red and blue spheres represent Al and Sm atoms, respectively. The arrows denote the displacement vectors. (For interpretation of the references to color in this figure legend, the reader is referred to the web version of this article.)

consequently the total ΔG is further split to

$$\Delta G = \Delta G_1 + \Delta G_2. \quad (4)$$

Here ΔG_1 and ΔG_2 represent the free energy barrier provided by either the natural thermal fluctuation or the WT-MetaD sampling, respectively. Consequently, the hopping time of a structural excitation event

$$\tau = \nu^{-1} = \tau_{\text{sampling}} \exp\left(\frac{\Delta G_2}{k_B T}\right), \quad (5)$$

where τ_{sampling} represents the *in silico* MD time as the correction term caused by the classical MD.

3. Results

3.1. Property differences of two model metallic glasses

We studied the relaxation dynamics and mechanical behaviors of $\text{Al}_{90}\text{Sm}_{10}$ and $\text{Y}_{65}\text{Cu}_{35}$ MGs by MD simulations. Fig. 2 shows the completely different relaxation and mechanical behaviors of the two MG systems. For $\text{Al}_{90}\text{Sm}_{10}$, there are three relaxation modes, in which the α relaxation and β relaxation are well separated from each other. This separation leads to the obvious β relaxation mode. However, for $\text{Y}_{65}\text{Cu}_{35}$, α and β relaxation are coupled with each other, leading to

the inconspicuous β relaxation compared to $\text{Al}_{90}\text{Sm}_{10}$. As shown in Fig. 2(b), the mechanical behaviors of these two MGs are also different. Compared with $\text{Y}_{65}\text{Cu}_{35}$, $\text{Al}_{90}\text{Sm}_{10}$ exhibits smaller yield strain, indicating that it is earlier to experience deformation.

3.2. Free energy sampling of $\text{Al}_{90}\text{Sm}_{10}$ MG

We demonstrate the free energy landscape and the long timescale collective atomic excitation mechanism in two prototypical model glasses by WT-MetaD. The typical examples of WT-MetaD samplings of the accelerated atoms with different w values in $\text{Al}_{90}\text{Sm}_{10}$ MG at 300 and 440 K are shown in Fig. 3. Fig. 3(a) shows two jumps in the CV trajectory except thermal fluctuation. The t_0 , t_1 and t_2 were labeled to represent the time of initial state, the first event and the second event, respectively. Note that t_1 and t_2 were selected as a period of time after the jump events occurred to guarantee a stable configuration. At t_0 , some ST atoms initially form a cluster, which is then accelerated by enhanced sampling. As the simulation proceeds, several accelerated atoms are activated and form an initial string. It is just the state corresponding to the first jump in the CV trajectory. After the first jump, the CV trajectory signals a second jump. The latter indicates that this nascent string continues to cooperatively move with the surrounding atoms, forming a long string together. The added bias potential is plotted in the inset of Fig. 3(c) as a function of CV.

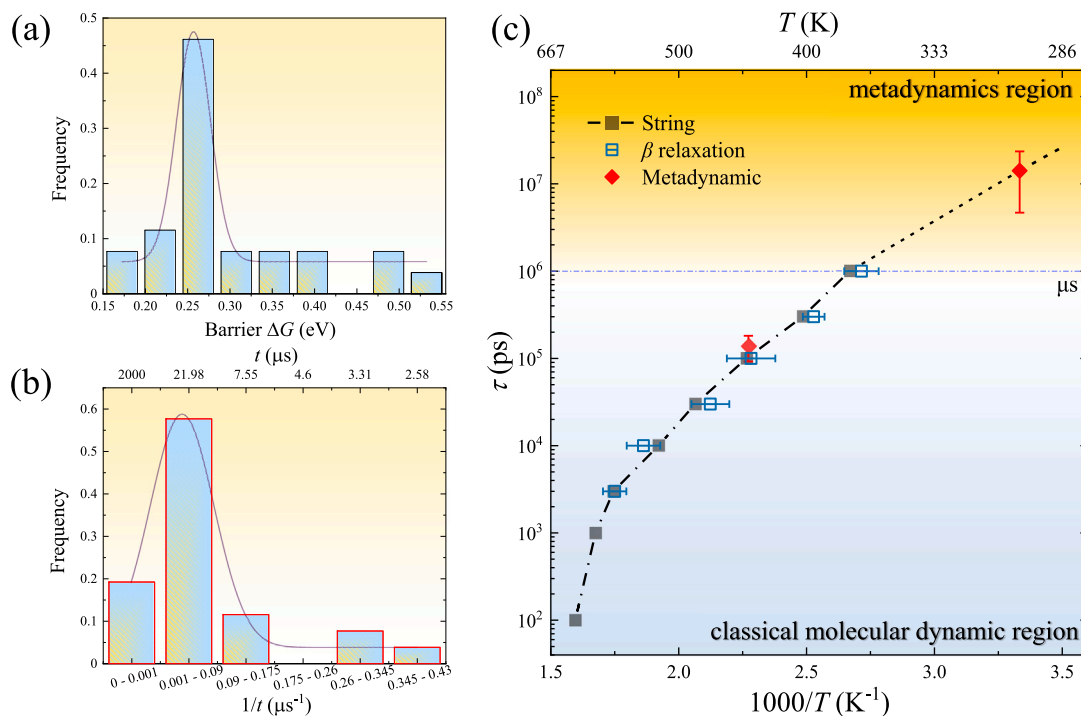


Fig. 4. (Color online) The statistical results of different ST atom clusters after samplings at 300 K of $\text{Al}_{90}\text{Sm}_{10}$ metallic glass. (a, b) Histogram of the free energy barrier ΔG_2 and the hopping incubation time of 26 selected events. (c) The β relaxation map of the $\text{Al}_{90}\text{Sm}_{10}$ metallic glass.

An analysis on the deposited Gaussians reproduces the original free energy surface, as shown in Fig. 3(c). It is worth mentioning that the free energy landscape shown in Fig. 3(c) is roughly the inverse plot of the outer envelope of the added bias potential during the WT-MetaD samplings, as shown in the inset of Fig. 3(c). The free energy landscape is actually the cumulative work done by the bias potential as it moves with variation of the CV. Local minima at 0.33, 0.93 and 1.24 \AA and a saddle point at 0.71 \AA demonstrate the validity of RMSD as a physically sound CV in describing this accelerated process. RMSD is thus a significant dimensionality reduction from the complicated path in the original $3N$ configuration. For the acceleration of the frozen atoms ($w = 0$) as shown in Fig. 3(b) and (d), the accelerated atoms show the same dynamic characteristics as those in ST atoms. Note that a remarkable difference is noticed in the two categories of accelerated atoms. Even if the temperature is increased from 300 to 440 K, the activation free energy of the frozen atoms is still several times larger than that of the ST atoms. This will lead to a gap of several orders of magnitude between the two events in timescale.

3.3. Quantifying the characteristic time of activation processes of ST atoms

To obtain more accurate and comprehensive free energy barrier ΔG_2 and the corresponding characteristic time of ST atoms after WT-MetaD sampling, we sample almost all the postulated ST clusters defined by large w value at 300 K and 440 K. Then, the estimated ΔG_2 and the characteristic times were statistically analyzed. Histograms of the free energy barrier ΔG_2 of the 26 independent samplings with different ST clusters at 300 K are shown in Fig. 4(a). The free energy barrier ΔG_2 of the ST atoms forming a string is estimated to be between 0.18 and 0.53 eV at 300 K. The hopping incubation time corresponding to this series of events can be obtained according to Eq. (4) and its distribution is shown in Fig. 4(b).

Considering the observation that ST atoms usually form string-like motions and both the string-like motions and STs are all closely related to the β relaxation, we compared the hopping incubation time of ST event via metadynamics with the characteristic time of the β

relaxation through MD-DMS, as well as the string-like motions obtained from classical MD. The energy barrier we obtained by metadynamics tends to be stable after such number of samplings (shown in Fig. S3 of SI). As shown in Fig. 4(c), the characteristic time of the string-like motions coincides with the β relaxation time. Furthermore, the hopping incubation time of the ST atom at 440 K is the same as classical MD. Extrapolating the characteristic time of the β relaxation and the string-like motions to low temperature region, as shown in Fig. 4(c), we find that the hopping incubation time obtained from WT-MetaD at ambient temperature (300 K) is consistent with classical MD. Note that at ambient temperature, the hopping timescale (~ 20 microsecond) is significantly beyond the limits of normal MD. In particular, these combined results mean that the hopping time obtained by WT-MetaD sampling is accurate and convincing while remains the atomic-scale detail. In the meantime, the accelerated ST atoms basically form string-like motions. The consistency of the characteristic time of ST, the β relaxation and the string-like motion indicates that they might share the same structural origin.

3.4. Free energy sampling of $\text{Y}_{65}\text{Cu}_{35}$ MG

To further study the correlation between ST and string-like motion, another MG system ($\text{Y}_{65}\text{Cu}_{35}$) with weak β relaxation was selected as a comparing reference. Meanwhile, most of the ST clusters in $\text{Y}_{65}\text{Cu}_{35}$ MG could not be successfully activated under the original metadynamic loading conditions, so we increased the width of the deposited Gaussian potential and bias temperature to 0.5 and 2500 in these cases, respectively. Even so, the frozen atoms in $\text{Y}_{65}\text{Cu}_{35}$ MG could not be successfully activated. Two typical examples of ST acceleration of $\text{Y}_{65}\text{Cu}_{35}$ MG at 300 K are shown in Fig. 5. Compared with $\text{Al}_{90}\text{Sm}_{10}$, the ST atoms in $\text{Y}_{65}\text{Cu}_{35}$ also exhibit the similar string-like motion and have approximately equal free energy barrier. However, such string-like motion only accounts for 20% of all the STs in $\text{Y}_{65}\text{Cu}_{35}$ case. The striking difference is that several atoms diffuse separately after the acceleration of the ST atoms in $\text{Y}_{65}\text{Cu}_{35}$ MG, while no cooperative motion is observed. This is a prevalent scenario in $\text{Y}_{65}\text{Cu}_{35}$, which

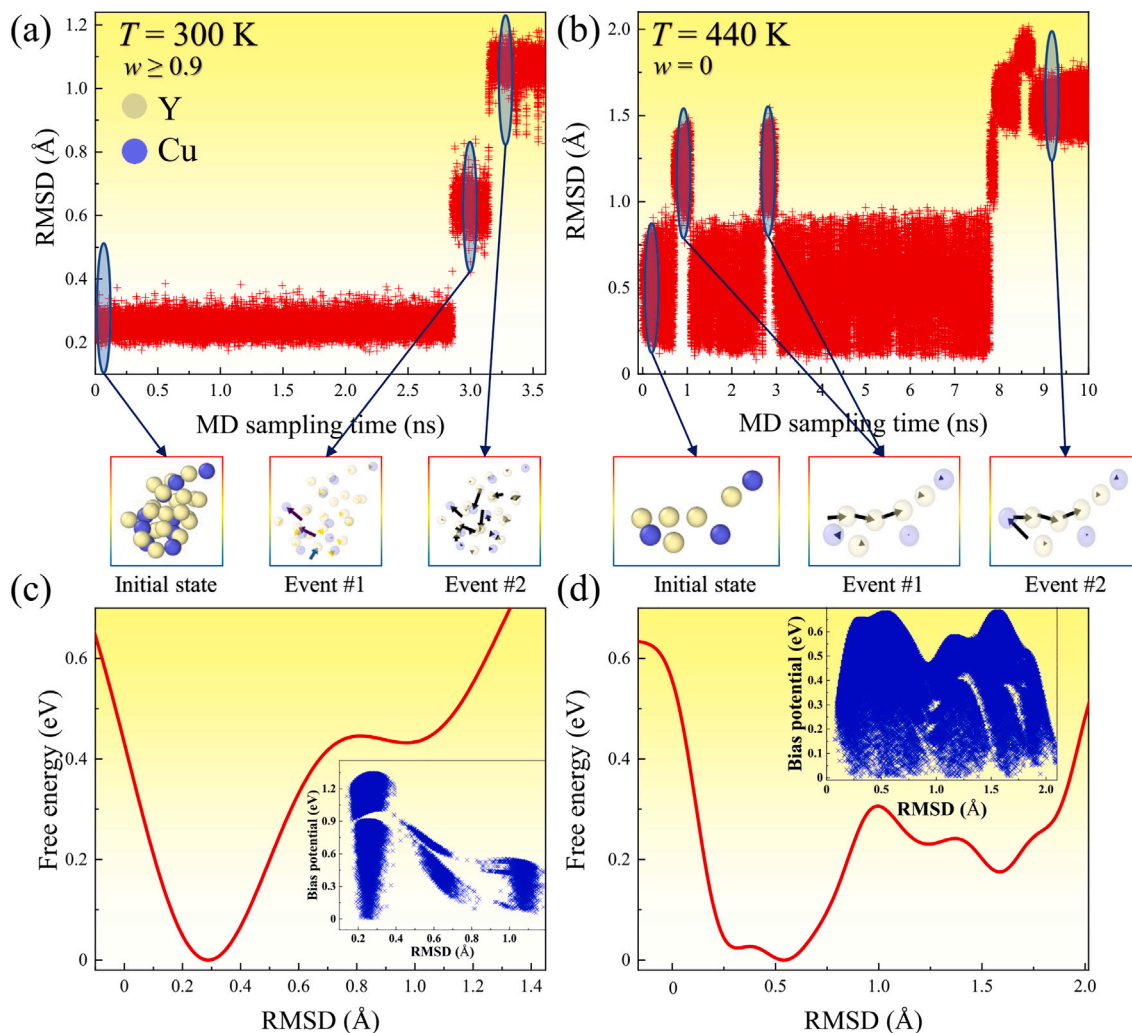


Fig. 5. Well-tempered metadynamics sampling of atomic rearrangement events in $Y_{65}Cu_{35}$ metallic glass. (a, b) Time evolution of RMSD. (c, d) Free energy profile versus RMSD. The inset shows the added bias potential. The middle panels show the initial state and the first two events, indicated by the sudden jump in CV. Yellow and blue spheres represent Al and Sm atoms, respectively. The arrows denote the displacement vectors. (For interpretation of the references to color in this figure legend, the reader is referred to the web version of this article.)

accounts for 50% of the rearrangement events. Compared with the string-like motion, their free energy barriers ΔG_2 are relatively larger in general.

3.5. Analyzing the influence of accelerated atoms on surrounding atoms

To clarify the difference in the basic atomic motion mechanism of these two MG systems, we analyzed the nonaffine displacement of the accelerated atoms as well as the surrounding atoms. As shown in Fig. 6, the acceleration of the ST atoms or the frozen atoms in $Al_{90}Sm_{10}$ both have significant impact on the surrounding atoms. These two kinds of atoms will eventually form a complete long string with the surrounding atoms. In particular, once some ST atoms and the frozen atom clusters in the potential string are accelerated, even if several atoms will diffuse separately, they will cooperatively move with the surrounding atoms and eventually form a complete string. In contrast, the ST atoms clusters have no effect on the surrounding atoms after excitation in $Y_{65}Cu_{35}$. Except for a small part of the chain formed within the cluster itself, most ST clusters show a phenomenon of free diffusion with a scattered atom pattern. We also tried to accelerate the frozen atoms in $Y_{65}Cu_{35}$, but they are hard to be excited and remain frozen under the premise of ensuring the accuracy of the WT-MetaD method.

4. Discussion

There are remarkable differences between the two investigated MGs according to the accelerated MD simulations. The influence of the accelerated atoms on the surrounding atoms is also quite distinct. To understand the microscopic causation for the differences, we analyzed the intrinsic structure of the two MGs. The distribution of w values reveals the structural origin of the effect of the accelerated atoms on the surrounding atoms. As shown in Fig. 7(a), most of the atoms in the $Y_{65}Cu_{35}$ MG are frozen, accounting for approximately 44% of the total number of atoms. With the increase in w value, the corresponding number of atoms constituting the potential ST gradually decreases. The number of frozen atoms in $Al_{90}Sm_{10}$ is significantly less than that of $Y_{65}Cu_{35}$, which only accounts for approximately 12% of the total number of atoms. The atoms in the range of $0 < w < 0.2$ account for the largest proportion, reaching 48% of the total number of atoms. The distribution of w in $Al_{90}Sm_{10}$ shows a peak, which also indicates the kinetic inhomogeneity of the $Al_{90}Sm_{10}$ compared with $Y_{65}Cu_{35}$. The cumulative probability density mapped in the illustration of Fig. 7(a) also shows the great difference in w values between these two MGs. To explain the structural differences between them more clearly, we project the three-dimensional atomic configuration to a two-dimensional demonstration to study the structural differences.

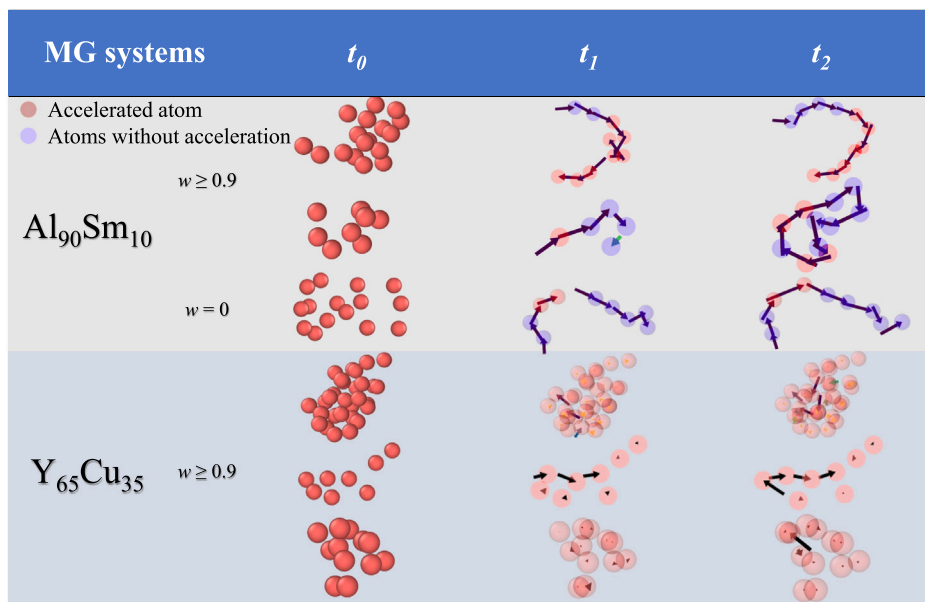


Fig. 6. The cooperative motion of the accelerated atoms and the surrounding atoms in $\text{Al}_{90}\text{Sm}_{10}$ and $\text{Y}_{65}\text{Cu}_{35}$ MGs. t_0 represents the initial configuration, t_1 and t_2 are the states after first and second jumps signaled by the CV trajectory after eliminating thermal fluctuation. The red and blue spheres represent the accelerated atoms and the surrounding atoms, respectively. (For interpretation of the references to color in this figure legend, the reader is referred to the web version of this article.)

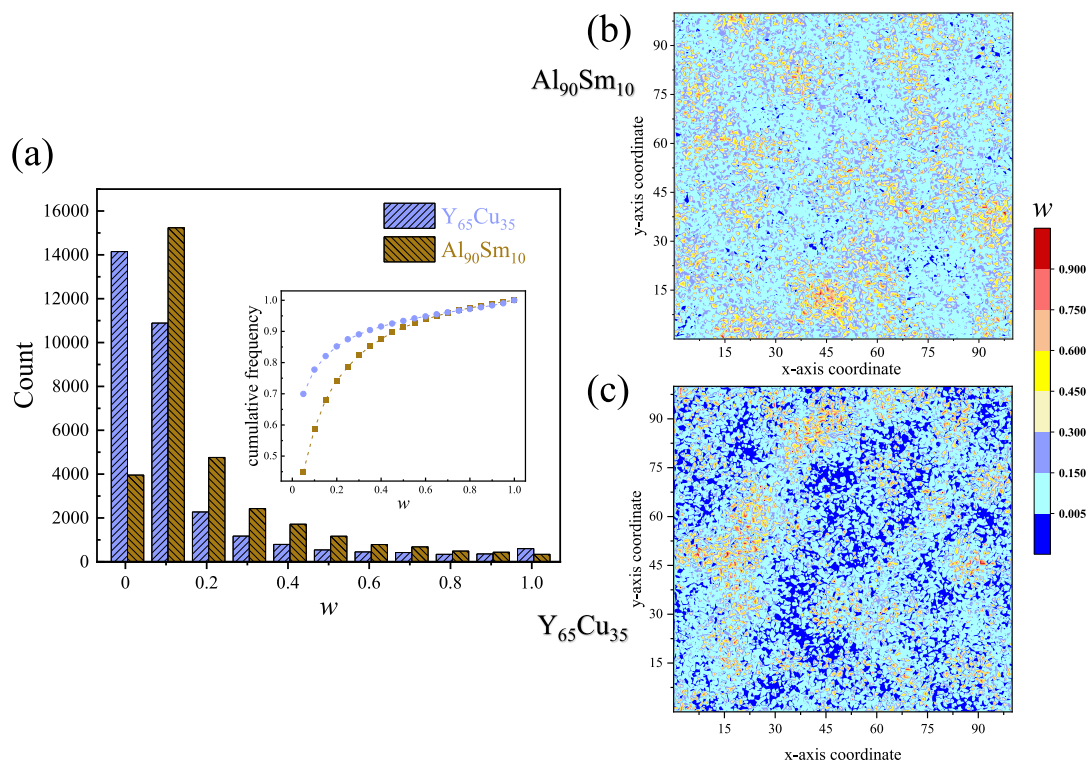


Fig. 7. (Color online) Structural difference analysis of two metallic glasses. (a) The distribution of w values in $\text{Al}_{90}\text{Sm}_{10}$ and $\text{Y}_{65}\text{Cu}_{35}$ MGs. (b, c) Two-dimensional schematic diagram of the structural difference between $\text{Al}_{90}\text{Sm}_{10}$ and $\text{Y}_{65}\text{Cu}_{35}$ metallic glass.

Figs. 7(b) and **7(c)** show the spatially structural difference of these two systems more intuitively. In $\text{Y}_{65}\text{Cu}_{35}$, the frozen area is relatively larger and evenly distributed. In comparison, the frozen area in $\text{Al}_{90}\text{Sm}_{10}$ is rather smaller and scattered. Meanwhile, by icosahedral and coordination number analysis, the atomic clusters with large w have poor symmetry, low number of immediately adjacent atoms, and are relatively loose (shown in Fig. S4 of SI and Fig. 8). Therefore, the larger the w value is, the softer the area. The relatively soft area represented by light blue is widely distributed. The environment of

$\text{Y}_{65}\text{Cu}_{35}$ is frozen atom region, which limits the movement of some fast-moving atoms. Finally, these fast-moving atoms are difficult to affect the surrounding atoms. Consequently, the cooperative movement is suppressed. This leads to the separation and diffusion of most atoms after once ST atoms clusters are activated in $\text{Y}_{65}\text{Cu}_{35}$. Similar to $\text{Al}_{90}\text{Sm}_{10}$, the separated and diffused atoms essentially have a tendency to cooperatively move with the surrounding atoms. Nonetheless, because of the restriction of its almost frozen environment in $\text{Y}_{65}\text{Cu}_{35}$, it is very difficult to form string-like motions. Some early strings formed

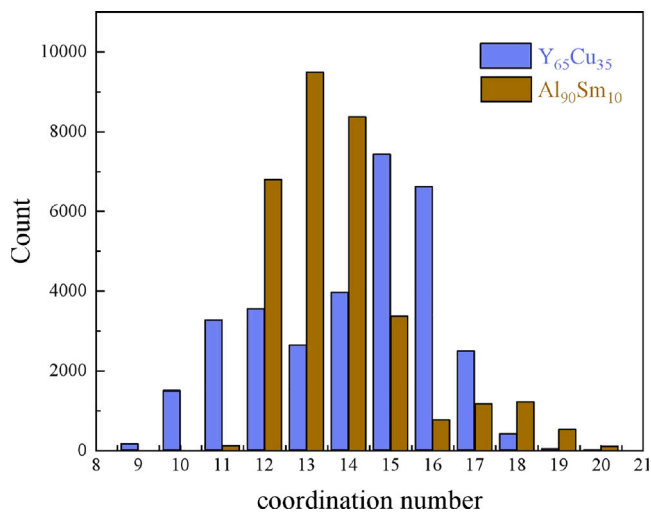


Fig. 8. (Color online) Coordination numbers analysis of two metallic glasses.

in the cluster have been significantly constrained. In Al₉₀Sm₁₀ MG, due to the relatively soft environment, the accelerated atoms are easily to be activated and can cooperatively move with the surrounding atoms after separation and diffusion, thus generating a large number of string-like motions. The atomic-scale observation is consistent with the experimental evidence for the superplastic deformation caused by large number of soft regions [20,98]. In Y₆₅Cu₃₅ MG, even if some frozen atoms will form strings together with the surrounding atoms, the activation energy of this chain movement formation is much larger and the corresponding characteristic time is longer. This string-forming behavior of the frozen atoms after acceleration can be interpreted to indicate that the frozen atoms can be activated to participate in the STs if the temperature has been raised sufficiently high in classical molecular dynamics or a large external force has been applied. As shown in Fig. 8, by analyzing the atomic coordination numbers of the two systems, we find that the Y₆₅Cu₃₅ MG has a larger number of atomic coordination numbers than the Al₉₀Sm₁₀ MG, indicating that the Y₆₅Cu₃₅ MG has more immediately adjacent atoms than the Al₉₀Sm₁₀ MG and is relatively compact. This also demonstrates that string-like motions are difficult to generate and extend in the Y₆₅Cu₃₅ MG.

5. Conclusions

In sum, by conducting molecular dynamics simulations under laboratory conditions, we capture the specific motion mechanism of the elementary unit of plastic deformation (ST). The atoms involved in the STs tend to form string-like motions. In some systems, due to their unique structural feature, such string-like motions are easily excited and not confined spatially, as in the case of Al₉₀Sm₁₀ MG, which exhibits a significant β relaxation feature. Such metallic glass is also easily deformed on a macroscopic scale. In other systems, such as Y₆₅Cu₃₅ MG, the string-like motion is suppressed by the large frozen environment. Therefore, the string-like collective motion is difficult to be excited and does not propagate, leading to a general lack of significant β relaxation and relatively less deformability at ambient temperature or at conventional time scales. Our simulations provide compelling atomic-scale ingredients to establish a fundamental link between ST, β relaxation and string-like motion, all of which are prevalent notions in amorphous solids but have never been unified. Therefore, the long-time-scale observation also supplies physical insight into the microscopic origin of plastic deformation in disordered materials. Finally, this work also highlights the importance of studying dynamics of glassy materials over long time scales that matters in the computational materials science and condensed matter physics.

Declaration of competing interest

The authors declare that they have no known competing financial interests or personal relationships that could have appeared to influence the work reported in this paper.

Acknowledgments

The computational work was supported by the public computing service platform provided by the Network and Computing Center of HUST, China. We are thankful for support from the National Science Foundation of China (NSFC 52071147 and 51601064) and the National Thousand Young Talents Program of China. Yun-Jiang Wang was supported by the NSFC (No. 12072344) and the Youth Innovation Promotion Association of the Chinese Academy of Sciences. Zhen-Ya Zhou was supported by the Ningxia Natural Science Foundation under Grant, China (2022AAC03066) and Ningxia Key Research and Development Program, China under Grant (2020BEB04026).

Appendix A. Supplementary data

Supplementary material related to this article can be found online at <https://doi.org/10.1016/j.actamat.2023.118701>.

References

- [1] W. Klement, R.H. Willens, P.O.L. Duwez, Non-crystalline structure in solidified gold-silicon alloys, *Nature* 187 (1960) 869–870.
- [2] A.L. Greer, *Metallic glasses*, Science 267 (1995) 1947–1953.
- [3] W.L. Johnson, Bulk glass-forming metallic alloys: Science and technology, *MRS Bull.* 24 (1999) 42–56.
- [4] W.H. Wang, C. Dong, C.H. Shek, Bulk metallic glasses, *Mater. Sci. Eng. R* 44 (2004) 45–89.
- [5] J. Pan, Q. Chen, L. Liu, Y. Li, Softening and dilatation in a single shear band, *Acta Mater.* 59 (2011) 5146–5158.
- [6] H. Tanaka, H. Tong, R. Shi, J. Russo, Revealing key structural features hidden in liquids and glasses, *Nat. Rev. Phys.* 1 (2019) 333–348.
- [7] H. Tong, H. Tanaka, Role of attractive interactions in structure ordering and dynamics of glass-forming liquids, *Phys. Rev. Lett.* 124 (2020) 225501.
- [8] Y. Sun, S.-X. Peng, Q. Yang, F. Zhang, M.-H. Yang, C.-Z. Wang, K.-M. Ho, H.-B. Yu, Predicting complex relaxation processes in metallic glass, *Phys. Rev. Lett.* 123 (2019) 105701.
- [9] F. Spaepen, Metallic glasses that harden under strain, *Nature* 578 (2020) 521–522.
- [10] J. Li, F. Spaepen, T.C. Hufnagel, Nanometre-scale defects in shear bands in a metallic glass, *Phil. Mag. A* 82 (2002) 2623–2630.
- [11] T. Rouxel, J. il Jang, U. Ramamurty, Indentation of glasses, *Prog. Mater. Sci.* 121 (2021) 100834.
- [12] S. Lan, L. Zhu, Z. Wu, L. Gu, Q. Zhang, H. Kong, J. Liu, R. Song, S. Liu, G. Sha, Y. Wang, Q. Liu, W. Liu, P. Wang, C.-T. Liu, Y. Ren, X.-L. Wang, A medium-range structure motif linking amorphous and crystalline states, *Nature Mater.* 20 (2021) 1347–1352.
- [13] Y.-C. Hu, H. Tanaka, Origin of the boson peak in amorphous solids, *Nat. Phys.* 18 (2022) 669–677.
- [14] Z.-Y. Yang, Y.-J. Wang, A. Zaccone, Correlation between vibrational anomalies and emergent anharmonicity of the local potential energy landscape in metallic glasses, *Phys. Rev. B* 105 (2022) 014204.
- [15] H. Zhang, C. Zhong, J.F. Douglas, X. Wang, Q. Cao, D. Zhang, J.-Z. Jiang, Role of string-like collective atomic motion on diffusion and structural relaxation in glass forming Cu-Zr alloys, *J. Chem. Phys.* 142 (2015) 164506.
- [16] J.F. Douglas, B.A. Pazmino Betancourt, X. Tong, H. Zhang, Localization model description of diffusion and structural relaxation in glass-forming Cu-Zr alloys, *J. Stat. Mech.-Theory Exp.* 2016 (2016) 054048.
- [17] P. Ross, S. Kuchemann, P.M. Derlet, H. Yu, W. Arnold, P. Liaw, K. Samwer, R. Maaß, Linking macroscopic rejuvenation to nano-elastic fluctuations in a metallic glass, *Acta Mater.* 138 (2017) 111–118.
- [18] P.M. Derlet, R. Maaß, J.F. Löffler, The boson peak of model glass systems and its relation to atomic structure, *Eur. Phys. J. B* 85 (2012) 148.
- [19] A. Inoue, B. Shen, H. Koshida, H. Kato, A.R. Yavari, Cobalt-based bulk glassy alloy with ultrahigh strength and soft magnetic properties, *Nature Mater.* 2 (2003) 661–663.
- [20] Y.H. Liu, G. Wang, R.J. Wang, D.Q. Zhao, M.X. Pan, W.H. Wang, Super plastic bulk metallic glasses at room temperature, *Science* 315 (2007) 1385–1388.
- [21] C.A. Schuh, T.C. Hufnagel, U. Ramamurty, Mechanical behavior of amorphous alloys, *Acta Mater.* 55 (2007) 4067–4109.

- [22] M. Chen, Mechanical behavior of metallic glasses: Microscopic understanding of strength and ductility, *Annu. Rev. Mater. Res.* 38 (2008) 445–469.
- [23] M.M. Trexler, N.N. Thadhani, Mechanical properties of bulk metallic glasses, *Prog. Mater. Sci.* 55 (2010) 759–839.
- [24] W.H. Wang, The elastic properties, elastic models and elastic perspectives of metallic glasses, *Prog. Mater. Sci.* 57 (2012) 487–656.
- [25] J. Schroers, Bulk metallic glasses, *Phys. Today* 66 (2013) 32–37.
- [26] J.C. Qiao, Q. Wang, D. Crespo, Y. Yang, J.M. Pelletier, Amorphous physics and materials: Secondary relaxation and dynamic heterogeneity in metallic glasses: A brief review, *Chin. Phys. B* 26 (2017) 016402.
- [27] J. Pan, Y.P. Ivanov, W.H. Zhou, Y. Li, A.L. Greer, Strain-hardening and suppression of shear-banding in rejuvenated bulk metallic glass, *Nature* 578 (2020) 559–562.
- [28] M. Ozawa, L. Berthier, G. Biroli, A. Rosso, G. Tarjus, Random critical point separates brittle and ductile yielding transitions in amorphous materials, *Proc. Natl. Acad. Sci.* 115 (2018) 6656–6661.
- [29] R. Maaß, P. Derlet, Micro-plasticity and recent insights from intermittent and small-scale plasticity, *Acta Mater.* 143 (2018) 338–363.
- [30] H.W. Sheng, W.K. Luo, F.M. Alamgir, J.M. Bai, E. Ma, Atomic packing and short-to-medium-range order in metallic glasses, *Nature* 439 (2006) 419–425.
- [31] A. Hirata, L.J. Kang, T. Fujita, B. Klumov, K. Matsue, M. Kotani, A.R. Yavari, M.W. Chen, Geometric frustration of icosahedron in metallic glasses, *Science* 341 (2013) 376–379.
- [32] E.D. Cubuk, R.J.S. Ivancic, S.S. Schoenholz, D.J. Strickland, A. Basu, Z.S. Davidson, J. Fontaine, J.L. Hor, Y.R. Huang, Y. Jiang, N.C. Keim, K.D. Koshigan, J.A. Lefever, T. Liu, X.G. Ma, D.J. Magagnosc, E. Morrow, C.P. Ortiz, J.M. Rieser, A. Shavit, T. Still, Y. Xu, Y. Zhang, K.N. Nordstrom, P.E. Arratia, R.W. Carpick, D.J. Durian, Z. Fakhraai, D.J. Jerolmack, D. Lee, J. Li, R. Riggleman, K.T. Turner, A.G. Yodh, D.S. Gianola, J. Liu Andrea, Structure-property relationships from universal signatures of plasticity in disordered solids, *Science* 358 (2017) 1033–1037.
- [33] V. Bapst, T. Keck, A. Grabska-Barwińska, C. Donner, E.D. Cubuk, S.S. Schoenholz, A. Obika, A.W.R. Nelson, T. Back, D. Hassabis, P. Kohli, Unveiling the predictive power of static structure in glassy systems, *Nat. Phys.* 16 (2020) 448–454.
- [34] A.S. Argon, Plastic deformation in metallic glasses, *Acta Metall.* 27 (1979) 47–58.
- [35] M.L. Falk, J.S. Langer, Dynamics of viscoplastic deformation in amorphous solids, *Phys. Rev. E* 57 (1998) 7192–7205.
- [36] C. Maloney, A. Lemaitre, Subextensive scaling in the athermal, quasistatic limit of amorphous matter in plastic shear flow, *Phys. Rev. Lett.* 93 (2004) 016001.
- [37] M.L. Falk, J.S. Langer, Deformation and failure of amorphous, solidlike materials, *Annu. Rev. Condens. Matter Phys.* 2 (2011) 353–373.
- [38] D. Şoşu, A. Stukowski, M. Stoica, S. Scudino, Atomic-level processes of shear band nucleation in metallic glasses, *Phys. Rev. Lett.* 119 (2017) 195503.
- [39] S. Torquato, Hard knock for thermodynamics, *Nature* 405 (2000) 521–523.
- [40] D. Rodney, C. Schuh, Distribution of thermally activated plastic events in a flowing glass, *Phys. Rev. Lett.* 102 (2009) 235503.
- [41] H.B. Yu, W.H. Wang, H.Y. Bai, Y. Wu, M.W. Chen, Relating activation of shear transformation zones to β relaxations in metallic glasses, *Phys. Rev. B* 81 (2010) 220201.
- [42] H.L. Peng, M.Z. Li, W.H. Wang, Structural signature of plastic deformation in metallic glasses, *Phys. Rev. Lett.* 106 (2011) 135503.
- [43] H.B. Yu, X. Shen, Z. Wang, L. Gu, W.H. Wang, H.Y. Bai, Tensile plasticity in metallic glasses with pronounced β relaxations, *Phys. Rev. Lett.* 108 (2012) 015504.
- [44] J. Büinz, T. Brink, K. Tsuchiya, F. Meng, G. Wilde, K. Albe, Low temperature heat capacity of a severely deformed metallic glass, *Phys. Rev. Lett.* 112 (2014) 135501.
- [45] Y.P. Mitrofanov, M. Peterlechner, S.V. Divinski, G. Wilde, Impact of plastic deformation and shear band formation on the boson heat capacity peak of a bulk metallic glass, *Phys. Rev. Lett.* 112 (2014) 135901.
- [46] P. Luo, P. Wen, H.Y. Bai, B. Ruta, W.H. Wang, Relaxation decoupling in metallic glasses at low temperatures, *Phys. Rev. Lett.* 118 (2017) 225901.
- [47] Q. Wang, J.J. Liu, Y.F. Ye, T.T. Liu, S. Wang, C.T. Liu, J. Lu, Y. Yang, Universal secondary relaxation and unusual brittle-to-ductile transition in metallic glasses, *Mater. Today* 20 (2017) 293–300.
- [48] Z.Y. Zhou, H.L. Peng, H.B. Yu, Structural origin for vibration-induced accelerated aging and rejuvenation in metallic glasses, *J. Chem. Phys.* 150 (2019) 204507.
- [49] Z.Y. Zhou, Q. Chen, Y. Sun, H.B. Yu, Unveiling correlation between α_2 relaxation and yielding behavior in metallic glasses, *Phys. Rev. B* 103 (2021) 094117.
- [50] G.-J. Lyu, J.-C. Qiao, Y. Yao, Y.-J. Wang, J. Morthomas, C. Fusco, D. Rodney, Microstructural effects on the dynamical relaxation of glasses and glass composites: A molecular dynamics study, *Acta Mater.* 220 (2021) 117293.
- [51] Y. Fan, T. Iwashita, T. Egami, How thermally activated deformation starts in metallic glass, *Nature Commun.* 5 (2014) 5083.
- [52] Y. Fan, T. Iwashita, T. Egami, Crossover from localized to cascade relaxations in metallic glasses, *Phys. Rev. Lett.* 115 (2015) 045501.
- [53] W.L. Johnson, K. Samwer, A universal criterion for plastic yielding of metallic glasses with a $(t/T_g)^{2/3}$ temperature dependence, *Phys. Rev. Lett.* 95 (2005) 195501.
- [54] J. Schroers, W.L. Johnson, Ductile bulk metallic glass, *Phys. Rev. Lett.* 93 (2004) 255506.
- [55] J.J. Lewandowski, W.H. Wang, A.L. Greer, Intrinsic plasticity or brittleness of metallic glasses, *Phil. Mag. Lett.* 85 (2005) 77–87.
- [56] J. Wang, D. Zhao, M. Pan, W. Wang, S. Song, T. Nieh, Correlation between onset of yielding and free volume in metallic glasses, *Scr. Mater.* 62 (2010) 477–480.
- [57] H. Wagner, D. Bedorf, S. Küchemann, M. Schwabe, B. Zhang, W. Arnold, K. Samwer, Local elastic properties of a metallic glass, *Nature Mater.* 10 (2011) 439–442.
- [58] D. Srolovitz, K. Maeda, V. Vitek, T. Egami, Structural defects in amorphous solids statistical analysis of a computer model, *Phil. Mag. A* 44 (1981) 847–866.
- [59] G.P. Johari, M. Goldstein, Viscous liquids and the glass transition. ii. secondary relaxations in glasses of rigid molecules, *J. Chem. Phys.* 53 (1970) 2372–2388.
- [60] H.B. Yu, R. Richert, K. Samwer, Structural rearrangements governing johari-goldstein relaxations in metallic glasses, *Sci. Adv.* 3 (2017) e1701577.
- [61] C. Donati, J.F. Douglas, W. Kob, S.J. Plimpton, P.H. Poole, S.C. Glotzer, Stringlike cooperative motion in a supercooled liquid, *Phys. Rev. Lett.* 80 (1998) 2338–2341.
- [62] T.B. Schröder, S. Sastry, J.C. Dyre, S.C. Glotzer, Crossover to potential energy landscape dominated dynamics in a model glass-forming liquid, *J. Chem. Phys.* 112 (2000) 9834–9840.
- [63] T. Kawasaki, A. Onuki, Dynamics of thermal vibrational motions and stringlike jump motions in three-dimensional glass-forming liquids, *J. Chem. Phys.* 138 (2013) 12A514.
- [64] P. Derlet, R. Maaß, Thermally-activated stress relaxation in a model amorphous solid and the formation of a system-spanning shear event, *Acta Mater.* 143 (2018) 205–213.
- [65] P. Derlet, R. Maaß, Thermal processing and enthalpy storage of a binary amorphous solid: A molecular dynamics study, *J. Mat. Res.* 32 (2017) 2668–2679.
- [66] F. Faupel, W. Frank, M.-P. Macht, H. Mehrer, V. Naundorf, K. Rätzke, H.R. Schöber, S.K. Sharma, H. Teichler, Diffusion in metallic glasses and supercooled melts, *Rev. Modern Phys.* 75 (2003) 237–280.
- [67] W. Ji, T.W.J. de Geus, M. Popović, E. Agoritsas, M. Wyart, Thermal origin of quasilocalized excitations in glasses, *Phys. Rev. E* 102 (2020) 062110.
- [68] P.M. Derlet, H. Bocquet, R. Maaß, Viscosity and transport in a model fragile metallic glass, *Phys. Rev. Mater.* 5 (2021) 125601.
- [69] P. Derlet, R. Maaß, Micro-plasticity in a fragile model binary glass, *Acta Mater.* 209 (2021) 116771.
- [70] D. Rodney, C.A. Schuh, Yield stress in metallic glasses: The jamming-jamming transition studied through monte carlo simulations based on the activation-relaxation technique, *Phys. Rev. B* 80 (2009) 184203.
- [71] S. Swayamjyoti, J.F. Löffler, P.M. Derlet, Local structural excitations in model glasses, *Phys. Rev. B* 89 (2014) 224201.
- [72] P. Koziatek, J.-L. Barrat, P. Derlet, D. Rodney, Inverse meyer-neldel behavior for activated processes in model glasses, *Phys. Rev. B* 87 (2013) 224105.
- [73] D. Rodney, A. Tanguy, D. Vandembroucq, Modeling the mechanics of amorphous solids at different length scale and time scale, *Modelling Simul. Mater. Sci. Eng.* 19 (2011) 083001.
- [74] A. Ninarello, L. Berthier, D. Coslovich, Models and algorithms for the next generation of glass transition studies, *Phys. Rev. X* 7 (2017) 021039.
- [75] A. Laio, M. Parrinello, Escaping free-energy minima, *Proc. Natl. Acad. Sci.* 99 (2002) 12562.
- [76] A. Kushima, X. Lin, J. Li, J. Eapen, J.C. Mauro, X. Qian, P. Diep, S. Yip, Computing the viscosity of supercooled liquids, *J. Chem. Phys.* 130 (2009) 224504.
- [77] L.K. Béland, P. Brommer, F. El-Mellouhi, J.-F. m. c. Joly, N. Mousseau, Kinetic activation-relaxation technique, *Phys. Rev. E* 84 (2011) 046704.
- [78] P. Cao, X. Lin, H.S. Park, Strain-rate and temperature dependence of yield stress of amorphous solids via a self-learning metabasin escape algorithm, *J. Mech. Phys. Solids* 68 (2014) 239–250.
- [79] P. Cao, M.P. Short, S. Yip, Understanding the mechanisms of amorphous creep through molecular simulation, *Proc. Natl. Acad. Sci.* 114 (2017) 13631.
- [80] P.M. Piaggi, O. Valsson, M. Parrinello, Enhancing entropy and enthalpy fluctuations to drive crystallization in atomistic simulations, *Phys. Rev. Lett.* 119 (2017) 015701.
- [81] M. Parrinello, A. Rahman, Polymorphic transitions in single crystals: A new molecular dynamics method, *J. Appl. Phys.* 52 (1981) 7182–7190.
- [82] A. Barducci, G. Bussi, M. Parrinello, Well-tempered metadynamics: A smoothly converging and tunable free-energy method, *Phys. Rev. Lett.* 100 (2008) 020603.
- [83] J.F. Dama, M. Parrinello, G.A. Voth, Well-tempered metadynamics converges asymptotically, *Phys. Rev. Lett.* 112 (2014) 240602.
- [84] Y.J. Wang, J.-P. Du, S. Shinzato, L.H. Dai, S. Ogata, A free energy landscape perspective on the nature of collective diffusion in amorphous solids, *Acta Mater.* 157 (2018) 165–173.
- [85] G. Bussi, A. Laio, Using metadynamics to explore complex free-energy landscapes, *Nat. Rev. Phys.* 2 (2020) 200–212.
- [86] Y.B. Yang, Q. Yang, D. Wei, L.H. Dai, H.B. Yu, Y.J. Wang, Unraveling strongly entropic effect on β -relaxation in metallic glass: Insights from enhanced atomistic samplings over experimentally relevant timescales, *Phys. Rev. B* 102 (2020) 174103.

- [87] S. Plimpton, Fast parallel algorithms for short-range molecular dynamics, *J. Comput. Phys.* 117 (1995) 1–19.
- [88] W.M. Brown, P. Wang, S.J. Plimpton, A.N. Tharrington, Implementing molecular dynamics on hybrid high performance computers – short range forces, *Comput. Phys. Comm.* 182 (2011) 898–911.
- [89] W.M. Brown, A. Kohlmeyer, S.J. Plimpton, A.N. Tharrington, Implementing molecular dynamics on hybrid high performance computers – particle–particle particle–mesh, *Comput. Phys. Comm.* 183 (2012) 449–459.
- [90] W.M. Brown, M. Yamada, Implementing molecular dynamics on hybrid high performance computers—three-body potentials, *Comput. Phys. Comm.* 184 (2013) 2785–2793.
- [91] Q. Wang, J.H. Li, J.B. Liu, B.X. Liu, Favored composition design and atomic structure characterization for ternary Al–Cu–Y metallic glasses via proposed interatomic potential, *J. Phys. Chem. B* 118 (2014) 4442–4449.
- [92] M.I. Mendeleev, F. Zhang, Z. Ye, Y. Sun, M.C. Nguyen, S.R. Wilson, C.Z. Wang, K.M. Ho, Development of interatomic potentials appropriate for simulation of devitrification of al90sm10alloy, *Modelling Simul. Mater. Sci. Eng.* 23 (2015) 045013.
- [93] H.B. Yu, M.H. Yang, Y. Sun, F. Zhang, J.B. Liu, C.Z. Wang, K.M. Ho, R. Richert, K. Samwer, Fundamental link between β relaxation, excess wings, and cage-breaking in metallic glasses, *J. Phys. Chem. Lett.* 9 (2018) 5877–5883.
- [94] A. Widmer-Cooper, P. Harrowell, H. Fynewever, How reproducible are dynamic heterogeneities in a supercooled liquid? *Phys. Rev. Lett.* 93 (2004) 135701.
- [95] A. Widmer-Cooper, H. Perry, P. Harrowell, D.R. Reichman, Irreversible reorganization in a supercooled liquid originates from localized soft modes, *Nat. Phys.* 4 (2008) 711–715.
- [96] G. Fiorin, M.L. Klein, J. Hénin, Using collective variables to drive molecular dynamics simulations, *Mol. Phys.* 111 (2013) 3345–3362.
- [97] H. Eyring, The activated complex in chemical reactions, *J. Chem. Phys.* 3 (1935) 107–115.
- [98] Y. Wu, D. Cao, Y. Yao, G. Zhang, J. Wang, L. Liu, F. Li, H. Fan, X. Liu, H. Wang, X. Wang, H. Zhu, S. Jiang, P. Kontis, D. Raabe, B. Gault, Z. Lu, Substantially enhanced plasticity of bulk metallic glasses by densifying local atomic packing, *Nature Commun.* 12 (2021) 6582.